ACS Catalysis

Research Article

pubs.acs.org/acscatalysis

Theoretical Investigation of the Reaction Mechanism of the Guaiacol Hydrogenation over a Pt(111) Catalyst

Jianmin Lu, Sina Behtash, Osman Mamun, and Andreas Heyden*

Department of Chemical Engineering, University of South Carolina, 301 South Main Street, Columbia, South Carolina 29208, United States

Supporting Information

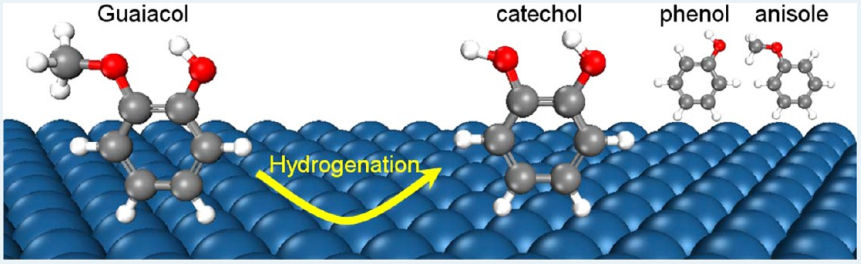

ABSTRACT: The reaction mechanism of the mild hydrogenation of guaiacol over Pt(111) has been investigated by density functional theory calculations and microkinetic modeling. Our model suggests that at 573 K, catechol is the preferred reaction product and that any deoxygenation to, for example, phenol or benzene is at least 4 orders of magnitude slower than the production of catechol. Slow deoxygenation of guaiacol can occur by decarbonylation and possibly by hydrogenation of the phenyl ring followed by C−OH bond cleavage. Direct −OH removal without activation of the phenyl ring is found to be at least 5 orders of magnitude slower. Overall, this study suggests that Pt(111) sites are not active deoxygenation sites and that the experimentally observed deoxygenation activity of Pt catalysts originates likely from the involvement of the catalyst support or Pt step and corner sites.

KEYWORDS: *guaiacol, platinum, density functional theory, microkinetic modeling, hydrotreatment, hydrodeoxygenation, biomass*

1. INTRODUCTION

Bio-oils derived from fast pyrolysis and hydrothermal liquefaction of lignocellulosic biomass are promising alternatives to depleting fossil fuels and have several environmental advantages. For instance, bio-oils are CO_2-neutral and emit no SO_x compounds and much less NO_x than, for example, diesel oil in a gas turbine.[1] Bio-oils are a complex mixture of water (15−30%) and several hundred organic compounds, including phenol derivatives (50−65%); lignin-derived oligomers (20%); and organic acids, aldehydes, alcohols, and esters.[2,3] The high content of oxygenated organic molecules leads to several disadvantages of bio-oils, such as high viscosity, high corrosiveness (acidity), instability, and low heating value, etc. To extend the possible applications of bio-oils, it is important to lower the oxygen concentration of bio-oils by proper upgrading strategies.

Catalytic upgrading of bio-oils is usually achieved by hydrotreatment (hydrogenation, hydrodeoxygenation, and dehydration), the key reaction of which is the C−O bond scission. Because bio-oils are a mixture of hundreds of organic compounds, model compounds are often studied in the search for better catalysts and to obtain a mechanistic understanding of the catalytic bio-oil upgrading process. Guaiacol, $C_6H_4(OH)(OCH_3)$, is a lignin building block that contains two oxygen-containing functional groups (−OH and $-OCH_3$) commonly found in the phenolic fraction of bio-oils. As a result, a considerable number of papers have reported an experimental investigation of the catalytic hydrogenation of guaiacol over monometallic transition metals, such as Fe,[4,5] Ni,[6] Ru,[6,7,5,8] Rh,[9,10,8] Pd,[6,9,5,8] and Pt,[11,9,12−14,5,8] and bimetallic catalysts, such as Co−Mo,[15] Pt−Sn,[16] Ni−Cu,[17] Rh−Pt,[9] and Pd−Fe.[5] As for Pt-based catalysts, three experimental studies stand out. Gutierrez el al.[9] have investigated the HDO of guaiacol over Pt/ZrO_2 at 100 °C in the presence of a high H_2 partial pressure (∼80 bar), and they observed cyclohexanol, 1-methyl-1,2-cyclohexanediol and 1,2-dimethoxy-benzene to be the major reaction products, suggesting a dominance of aromatic ring saturation. No reaction mechanism for the deoxygenation has been proposed by the authors. Next, Nimmanwudipong and co-workers[13] have suggested a reaction network for the hydrodeoxygenation (HDO) of guaiacol over $Pt/\gamma\text{-}Al_2O_3$ at 300 °C and low H_2 pressure (∼0.4 bar) on the basis of selectivity-conversion data. They conclude that the dominant deoxygenation pathway proceeds by the $-OCH_3$ removal of guaiacol to produce phenol, and catechol is mainly from $-CH_3$ removal of guaiacol. Finally, Sun and co-workers[5] have studied the HDO mechanism of guaiacol over various transition metal catalysts on carbon supports and proposed the following

Received: October 21, 2014
Revised: March 3, 2015
Published: March 10, 2015

DOI: 10.1021/cs5016244
ACS Catal. 2015, 5, 2423−2435

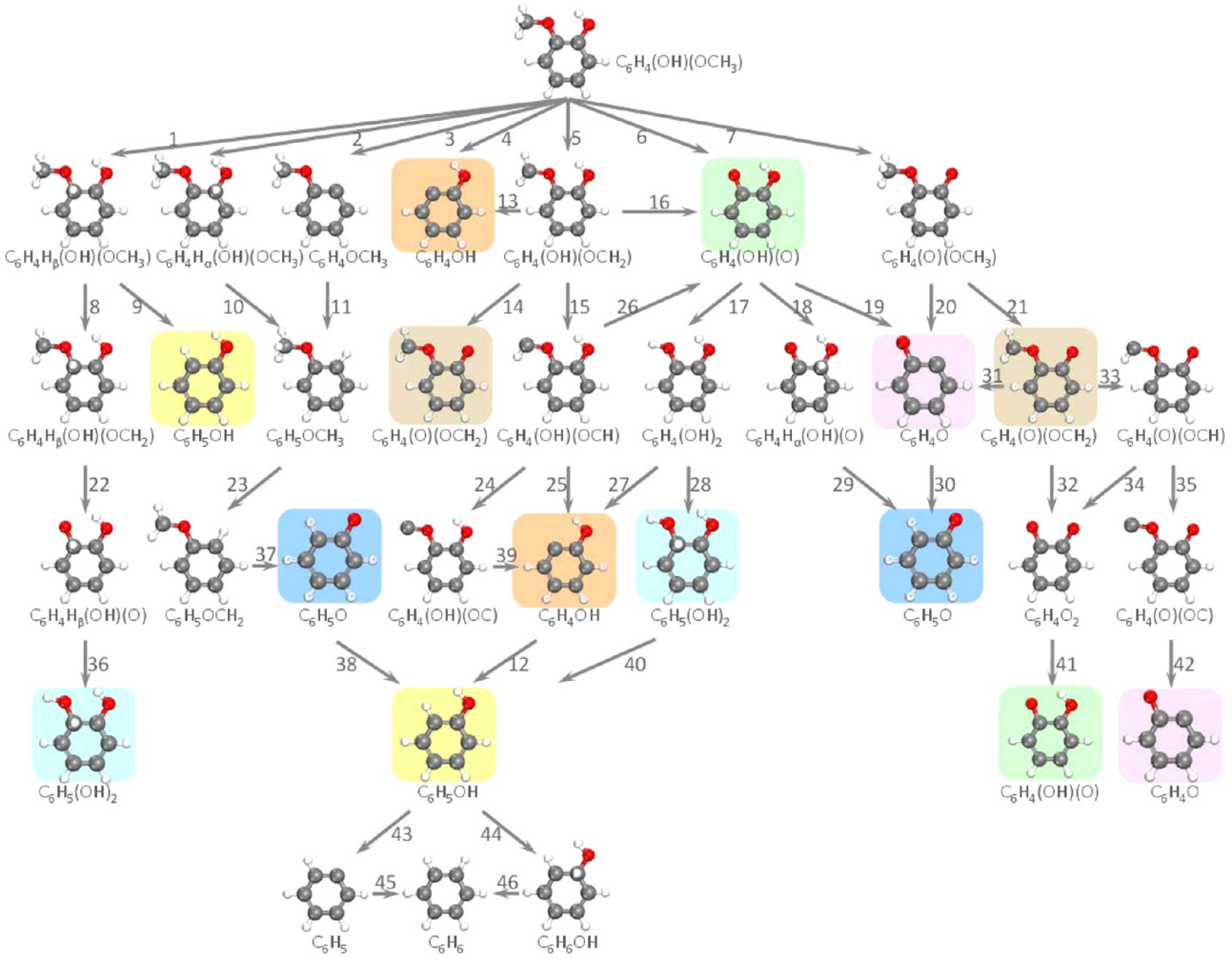

Figure 1. Reaction network investigated for the hydrogenation of guaiacol to aromatic products over Pt(111). For clarity, duplicate structures are highlighted by identical background colors.

reaction pathways on the basis of the reaction products: guaiacol → catechol → phenol → benzene for Ru, Pd, and Pt catalysts, and guaiacol → phenol → benzene for Fe and Pd−Fe catalysts.

Theoretical calculations based on first principles such as density functional theory (DFT) have become powerful tools for shedding more light on the reaction mechanism on transition metal surfaces; however, no theoretical report has yet been published on the hydrodeoxygenation of guaiacol to phenol and benzene over Pt-based catalysts. It is the objective of this study to investigate the hydrogenation pathways of guaiacol to aromatic products over Pt(111) model surfaces from first principles. We performed a comprehensive DFT study of various hydrogenation, dehydrogenation, and decomposition pathways and built a microkinetic model containing all of the pathways to identify the dominant mechanism under realistic reaction conditions. We note that this study is limited to Pt(111) sites and that more under-coordinated step or corner sites of metal nanopartilces[18,19] or an oxide support[20] have been proposed to also play an important role in the HDO of bio-oils. We will consider the importance of these sites in a future study. Finally, during the revision process of this paper, Lee et al. published a computational study for the hydrogenation of guaiacol to catechol over Pt(111), which contains a subset of the elementary reactions studied here.[21] Overall, their DFT results are very similar to our results; however, no microkinetic analysis has been performed by these authors.

2. COMPUTATIONAL METHODS

Periodic DFT calculations have been performed using the Vienna Ab Initio Simulation Package (VASP).[22,23] The projector-augmented wave (PAW) method was used to capture the electron−ion interactions. The PAW method is a frozen core all-electron method that uses the exact shape of the valence wave functions instead of pseudowave functions.[24] The exchange correlation energy has been calculated within the generalized gradient approximation (GGA) using the PBE functional.[25,26] An energy cutoff for the plane waves of 400 eV was employed throughout this study. For dispersion interactions, we used the DFT-D3 methodology.[27]

This level of theory computes a lattice constant of 3.9281 Å for bulk FCC-Pt, which is in reasonable agreement with the experimental value (3.9239 Å[28]). This lattice constant is used to construct a periodic Pt(111) slab with 4 Pt layers separated by a vacuum layer of 15 Å to eliminate interactions between the slab and its images. In total, there are 64 atoms in the slab, and each Pt layer has 16 Pt atoms with a $(4 \times 2\sqrt{3})$ periodicity, allowing for adsorbate coverages as low as 1/16 ML. The bottom two Pt layers are fixed to their optimized bulk configuration during all computations, and the top two layers and surface intermediates

DOI: 10.1021/cs5016244
ACS Catal. 2015, 5, 2423−2435

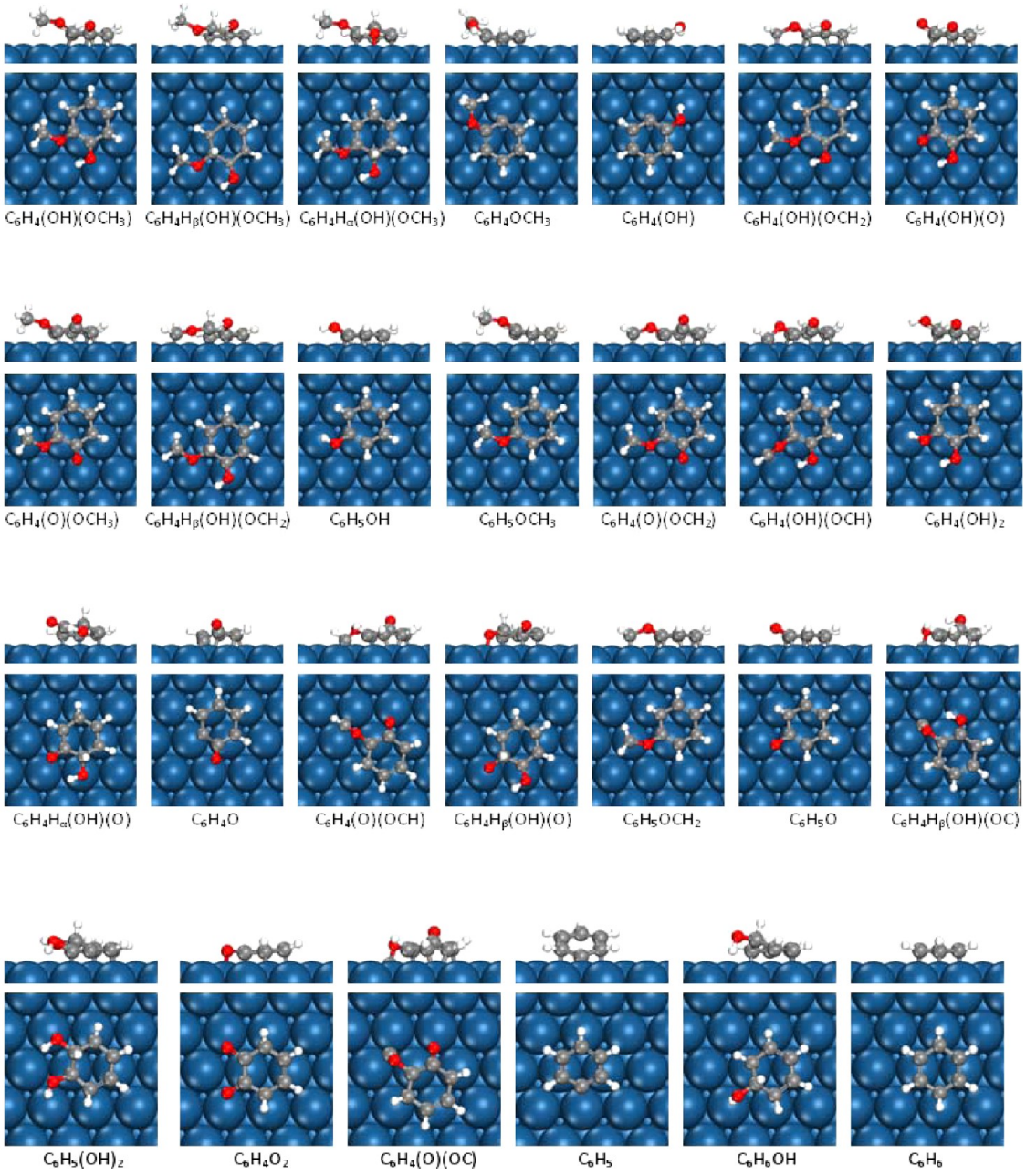

Figure 2. Side (upper panel) and top view (lower panel) of preferred adsorption structure of various intermediates with aromatic rings in the reaction network of the hydrogenation of guaiacol over Pt(111).

are fully relaxed. All atomic coordinates of the adsorbates and the Pt atoms in the relaxed layers are optimized to a force of <0.03 eV/Å on each atom. All self-consistent field calculations are converged to 1×10^{-5} kJ/mol. Brillouin zone integration is performed using a $4 \times 4 \times 1$ Monkhorst–Pack grid and a Methfessel–Paxton smearing of 0.2 eV.

Adsorption energies of all surface intermediates reported in this paper are calculated in their most favorable adsorption configuration. Adsorption energies, E_{ads}, are calculated as

$$E_{ads} = E_{slab+adsorbate} - E_{slab} - E_{adsorbate(gas)} \quad (1)$$

where $E_{slab+adsorbate}$ is the total energy of the Pt slab with an adsorbate bound to it, E_{slab} is the total energy of the clean Pt slab, and $E_{adsorbate(gas)}$ is the total energy of the adsorbate in the gas phase. Next, transition states for elementary reaction steps are determined by a combination of the nudged elastic band (NEB) method[29] and the dimer method.[30−32] In the NEB method, the path between the reactant and product is discretized into a series of structural images. The image closest to a likely transition state structure is used as an initial guess structure for the dimer method.

In the microkinetic model development, we have employed the same methodology already described in our previous paper.[33] Briefly, we solve the nonlinear equations resulting from a steady state reaction model with differential conversion using the BzzMath library[34] developed by G. Buzzi-Ferraris.

3. RESULTS AND DISCUSSION

Figure 1 illustrates the reaction pathways included for the HDO of guaiacol to aromatic products over the flat Pt(111) surface. It

DOI: 10.1021/cs5016244
ACS Catal. 2015, 5, 2423−2435

is noted that reaction pathways leading to (oxygenated) cycloalkanes have not been considered in this study. Figure S2 in the Supporting Information shows that at a typical experimental HDO reaction temperature of 573 K, the hydrogenation of the phenyl ring is thermodynamically not possible.

3.1. Adsorbed Intermediates. Adsorption geometries of the reactants, products, and possible intermediates involved in the reaction network are shown in Figure 2 and for smaller molecular fragments in the Supporting Information (Figure S3). The number of adsorption sites, adsorption energies and zero-point energy corrections of these intermediates are listed in Table 1. All adsorption energies and activation barriers reported in this study are zero-point energy corrected (ΔZPE).

All aromatic molecules considered can adsorb at four different adsorption sites (atop, bridge, fcc and hcp) on the Pt(111) surface with two orientations of 0° and 30° at each site, referring to the angles of the C−C bond relative to the close-packed metal−metal bond, as shown in Figure 3. Our calculations suggest that all 27 aromatic surface intermediates prefer to adsorb on the bridge 30° site. Liu et al. predicted the same chemisorbed benzene structure for the (111) surfaces of Pt, Pd, Ir, and Rh.[35] Stable aromatic intermediates such as guaiacol, anisole, catechol, phenol, and benzene, have adsorption energies of approximately −2.3 eV. As expected, in the gas phase, unstable aromatic intermediates bind to the surface much more strongly, dependingt on the degree of unsaturation. For example, the intermediate $C_6H_4(OH)(OCH_2)$ has an adsorption energy of −4.18 eV, and the intermediate $C_6H_4(OH)(OCH)$ has an adsorption energy of −5.46 eV.

3.3. Potential Energy Surfaces for Various Reaction Pathways. Various elementary steps have been included in the investigated reaction network shown in Figure 1. It is noted, though, that we did not consider hydrogenation pathways of the phenyl ring leading to saturated products, such as cyclohexanone and cyclohexanol. Although these reaction products have been observed at higher hydrogen partial pressures and lower temperatures, they are usually not desirable and are not the main reaction products over Pt catalysts at low H_2 partial pressures and temperatures above 573 K.[5] In the following, we labeled the reaction pathways (1−7) according to the first reaction step labeled step 1 to 7 in Figure 1. In our nomenclature, the phenyl ring carbon bound to the −OH group in the guaiacol molecule is symbolized the α carbon, and the phenyl ring carbon bound to the $-OCH_3$ group is called the β carbon. The seven reaction pathways investigated can be divided into three groups. The first group involves reaction pathways 1 and 2 that start with β and α carbon hydrogenation steps of the phenyl ring to activate the phenyl(C)−O bond. The second group involves reaction pathways 3, 4, and 6 that start with direct −OH, $-OCH_3$, and $-CH_3$ removal of guaiacol, respectively. Finally, the third group involves pathway 5, starting with dehydrogenation of the $-OCH_3$ group of guaiacol, and pathway 7, starting with dehydrogenation of the −OH group. All zero-point-energy-corrected reaction energies and activation barriers for all surface elementary steps investigated are listed in Table 2. Snapshots of transition state structures of all elementary steps are shown in the Supporting Information, Figures S4 and S5. We note that for the transition states of steps 3, 4, 13, 19, 20, 25, 27, 31, and 37, no dimer calculations could be converged (only the NEB), and the activation barriers for these steps are more approximate.

Table 1. Number of Adsorption Sites, Zero-Point Energy Corrected Adsorption Energies (E_{ads}, in eV), and Zero-Point Energy Corrections (ΔZPE, in eV) of All Reaction Intermediates on Pt(111) Computed by PBE-D3[a]

formula	no. sites	E_{ads} (eV)	ΔZPE (eV)
$C_6H_4(OH)(OCH_3)$, guaiacol	4	−2.27	0.02
$C_6H_4H_\beta(OH)(OCH_3)$	4	−3.59	0.04
$C_6H_4H_\alpha(OH)(OCH_3)$	4	−3.44	0.06
$C_6H_4OCH_3$	4	−3.41	0.03
C_6H_4OH	4	−3.48	0.00
$C_6H_4(OH)(OCH_2)$	5	−4.11	0.07
$C_6H_4(OH)(O)$	4	−2.94	0.02
$C_6H_4(O)(OCH_3)$	4	−3.05	0.00
$C_6H_4H_\beta(OH)(OCH_2)$	5	−4.76	0.13
$C_6H_5OCH_3$, anisole	4	−2.31	0.04
$C_6H_4(OH)(OCH)$	5	−5.40	0.06
$C_6H_4(OH)(OC)$	5	−5.57	0.06
$C_6H_4(OH)_2$, catechol	4	−2.39	0.01
C_6H_4O	4	−4.11	0.14
$C_6H_4(O)(OCH_2)$	5	−4.19	0.03
$C_6H_4(O)(OCH)$	5	−5.93	0.09
$C_6H_4(O)(OC)$	5	−3.47	−0.03
$C_6H_5OCH_2$	5	−4.02	0.09
C_6H_5O, phenoxy	4	−3.37	0.04
C_6H_5OH, phenol	4	−2.24	0.02
$C_6H_5(OH)_2$	5	−3.79	0.04
$C_6H_4O_2$	6	−2.91	−0.01
C_6H_5	4	−3.30	0.05
C_6H_6OH	4	−3.93	0.05
C_6H_6, benzene	4	−2.14	0.04
$C_6H_4H_\alpha(OH)(O)$	5	−2.64	0.06
H	1	−2.67	0.15
OH	1	−2.38	0.14
H_2O	1	−0.40	0.08
CH	1	−6.81	0.21
CH_2	1	−4.12	0.21
CH_3	1	−2.16	0.17
CH_4	1	−0.26	0.03
CO	1	−2.02	0.06
CHO	1	−2.59	0.14
CH_2O	2	−0.73	0.07
CH_3O	1	−1.82	0.14
CH_3OH	1	−0.63	0.06

[a]Herein, α carbon means the aromatic ring carbon binding to the −OH group and β carbon means the aromatic ring carbon binding to the $-OCH_3$ group. H_α symbolizes a hydrogen atom binding to the α carbon and H_β symbolizes a hydrogen atom binding to the β carbon.

However, out of these transition states, only step 37 possesses a reaction barrier below 1.4 eV and is therefore potentially kinetically accessible (most barriers are larger than 2.0 eV). Step 37 is on the reaction pathway to produce phenol; however, it is not rate-controlling on this pathway such that we do not expect our conclusions to change if more accurate transition state energies could be obtained.

3.3.1. Pathways involving hydrogenations of the phenyl ring. In the first pathway, the initial hydrogenation of the β carbon in guaiacol to form $C_6H_4H_\beta(OH)(OCH_3)$ (step 1) is kinetically demanding, with an activation barrier of 1.23 eV. Considering, furthermore, that this elementary step is endothermic by 0.55 eV, pathway 1 becomes kinetically accessible only at high temperatures. $C_6H_4H_\beta(OH)(OCH_3)$

DOI: 10.1021/cs5016244
ACS Catal. 2015, 5, 2423−2435

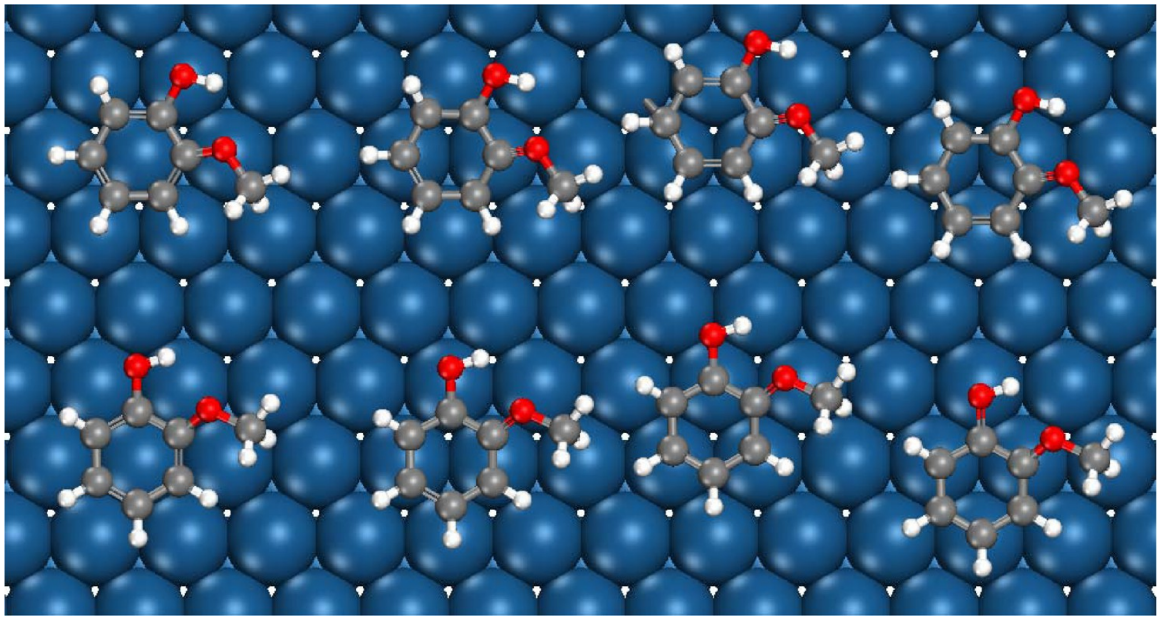

Figure 3. Illustration of adsorption sites for guaiacol on the Pt(111) surface. There are four possible adsorption sites—atop, bridge, fcc, and hcp. At each site, guaiacol has two orientations, 0° and 30°, referring to the angles of the C−C bond to the nearest-neighboring Pt−Pt bond.

can subsequently either go through dehydrogenation steps of the methoxy group to $C_6H_4H_\beta(OH)(OCH_2)$ (step 8) or go through a $-OCH_3$ removal step to produce phenol (step 9). Considering that both steps are approximately thermoneutral and that the barrier for step 8 is only 0.15 eV lower than the 1.00 eV barrier of step 9, both pathways are possible (we will show in section 3.4 that phenol production is preferred). Next, the methylene group ($-CH_2$) can be removed from $C_6H_4H_\beta(OH)(OCH_2)$ to form $C_6H_4H_\beta(OH)(O)$ (step 22), which is again a relatively difficult thermoneutral step with a barrier of 0.99 eV. Subsequent exothermic hydrogenation (ΔE_0 = −0.43 eV) of $C_6H_4H_\beta(OH)(O)$ to $C_6H_5(OH)_2$ (step 36) is rather easy, with a barrier of only 0.46 eV. Finally, the dehydroxylation to form phenol (step 40) is endothermic by 0.19 eV and has a barrier of 0.99 eV, such that we can conclude that pathway 1 is likely not viable at lower temperatures for the production of phenol, primarily because of the initial hydrogenation barrier of step 1 of 1.23 eV.

In pathway 2, the α carbon in guaiacol is hydrogenated to $C_6H_4H_\alpha(OH)(OCH_3)$ (step 2). We found for this highly endothermic process (ΔE_0 = 0.76 eV) an activation barrier of 1.03 eV, which is slightly lower than the activation barrier of the β carbon (see above), suggesting that this pathway might be preferred to the first pathway. $C_6H_4H_\alpha(OH)(OCH_3)$ can subsequently be dehydroxylated to form anisole (step 10), which is a mildly exothermic reaction (ΔE_0 = −0.10 eV) with a low activation barrier of 0.62 eV. Next, anisole can either desorb or follow a dehydrogenation step of the methoxy group to $C_6H_5OCH_2$ (step 23). This step is again exothermic (ΔE_0 = −0.39 eV) and possesses a kinetically accessible activation barrier of 0.79 eV. Methylene ($-CH_2$) removal of $C_6H_5OCH_2$ to phenoxy (step 37) is a difficult thermoneutral process with a barrier of 0.93 eV. Finally, phenoxy can get hydrogenated (step 38), which is a thermoneutral reaction with a low activation barrier of 0.29 eV. The α-carbon hydrogenation of anisole to $C_6H_5H_\alpha OCH_3$ is endothermic by 0.49 eV and has an activation barrier of 1.28 eV. Methoxy removal of $C_6H_5H_\alpha OCH_3$ to benzene is thermoneutral (0.04 eV) but needs to overcome a barrier of 1.04 eV. Considering the large activation barriers, we did not include this pathway in our microkinetic model.

We note that other reaction pathways, such as removal of the $-OCH_2$ group from $C_6H_5OCH_2$ followed by hydrogenation to benzene or further dehydrogenation of the methylene group of $C_6H_5OCH_2$ and subsequent −OCH or −OC removal, etc., are also, in principle, possible. However, since we will show in sections 3.3.3 and 3.4 that methylene removal from $C_6H_4(OH)(OCH_2)$ is preferred and we expect this to be also the case for $C_6H_5OCH_2$, we did not further study these pathways. In this context, it is noted that because of the high initial hydrogenation barrier of the phenyl ring of over 1.03 eV, pathway 2 is likely not viable at lower temperatures for the production of phenol. Finally, we note that we assumed in this Article that a "fast" reaction pathway exists for the isomerization of a hydrogenated phenyl ring structure with an H atom close to the Pt(111) surface (the structure formed during hydrogenation) and the corresponding structure with the H atom pointing away from the surface. Although we could not identify such a pathway in this study, we show in the Supporting Information that a pathway with a barrier of 1.58 eV exists. If, indeed, no pathway exists for this isomerization reaction with a lower activation barrier (>1 eV; facilitated by, e.g., adsorbed water), all deoxygenation pathways involving the hydrogenation of the phenyl ring become very slow.

3.3.2. Reaction Pathways Starting with Direct Removal of a Functional Group. In the following, we will show that direct removal of a functional group such as −OH, $-OCH_3$, and $-CH_3$ from guaiacol is also kinetically difficult because the guaiacol molecule is not sufficiently activated for these difficult C−O bond scissions on Pt(111). For example, in pathway 3, the direct removal of the −OH group in guaiacol to form $C_6H_4OCH_3$ (step 3) is a very slow endothermic process (ΔE_0 = 1.50 eV) with an activation barrier of 2.27 eV. Although the subsequent exothermic hydrogenation step (ΔE_0 = −0.84 eV) to anisole (step 11) has a barrier of only 0.75 eV, pathway 3 cannot be considered a viable deoxygenation pathway of guaiacol. Next, in pathway 4, the direct removal of the methoxy

DOI: 10.1021/cs5016244
ACS Catal. 2015, 5, 2423−2435

Table 2. Calculated Zero-Point-Corrected Reaction Energies (ΔE_0), Activation Barriers ($E^\dagger$), and Rate Parameters for All Elementary Reaction Steps Included in the Microkinetic Model of the Hydrogenation of Guaiacol over Pt(111)

			T (K)			
step	reaction	constant	473	523	573	623
0	$C_6H_4(OH)(OCH_3)$(gas) + 4* → $C_6H_4(OH)(OCH_3)$****	K_0	6.59×10^{6}	7.36×10^{3}	2.17×10^{1}	1.33×10^{-1}
	ΔE_0 = −2.27 eV	k_0^+, s^{-1} bar^{-1}	7.27×10^{7}	6.91×10^{7}	6.60×10^{7}	6.33×10^{7}
1	$C_6H_4(OH)(OCH_3)$**** + H* → $C_6H_4H_\beta(OH)(OCH_3)$**** + *	K_1	8.06×10^{-7}	2.72×10^{-6}	7.35×10^{-6}	1.68×10^{-5}
	ΔE_1 = 0.55 eV, $E_1^\dagger$ = 1.23 eV	k_1^+, s^{-1}	1.13	2.17×10^{1}	2.48×10^{2}	1.93×10^{3}
2	$C_6H_4(OH)(OCH_3)$**** + H* → $C_6H_4H_\alpha(OH)(OCH_3)$**** + *	K_2	3.02×10^{-9}	1.65×10^{-8}	6.64×10^{-8}	2.12×10^{-7}
	ΔE_2 = 0.76 eV, $E_2^\dagger$ = 1.03 eV	k_2^+, s^{-1}	8.38×10^{1}	9.97×10^{2}	7.70×10^{3}	4.28×10^{4}
3	$C_6H_4(OH)(OCH_3)$**** + * → $C_6H_4OCH_3$**** + OH*	K_3	1.75×10^{-16}	6.29×10^{-15}	1.22×10^{-13}	1.47×10^{-12}
	ΔE_3 = 1.50 eV, $E_3^\dagger$ = 2.27 eV	k_3^+, s^{-1}	8.30×10^{-12}	1.90×10^{-9}	1.69×10^{-7}	7.40×10^{-6}
4	$C_6H_4(OH)(OCH_3)$**** + * → C_6H_4OH**** + CH_3O*	K_4	3.83×10^{-13}	7.18×10^{-12}	8.12×10^{-11}	6.25×10^{-10}
	ΔE_4 = 1.22 eV, $E_4^\dagger$ = 2.14 eV	k_4^+, s^{-1}	1.84×10^{-10}	3.06×10^{-8}	2.11×10^{-6}	7.40×10^{-5}
5	$C_6H_4(OH)(OCH_3)$**** + 2* → $C_6H_4(OH)(OCH_2)$***** + H*	K_5	2.32×10^{4}	6.84×10^{3}	2.51×10^{3}	1.09×10^{3}
	ΔE_5 = −0.50 eV, $E_5^\dagger$ = 0.71 eV	k_5^+, s^{-1}	3.30×10^{4}	1.81×10^{5}	7.44×10^{5}	2.45×10^{6}
6	$C_6H_4(OH)(OCH_3)$**** + * → $C_6H_4(OH)(O)$**** + CH_3*	K_6	2.50×10^{6}	6.64×10^{5}	2.23×10^{5}	8.99×10^{4}
	ΔE_6 = −0.58 eV, $E_6^\dagger$ = 2.00 eV	k_6^+, s^{-1}	1.70×10^{-8}	2.22×10^{-6}	1.25×10^{-4}	3.74×10^{-3}
7	$C_6H_4(OH)(OCH_3)$**** + * → $C_6H_4(O)(OCH_3)$**** + H*	K_7	1.23×10^{-1}	1.51×10^{-1}	1.79×10^{-1}	2.08×10^{-1}
	ΔE_7 = 0.08 eV, $E_7^\dagger$ = 0.37 eV	k_7^+, s^{-1}	3.70×10^{8}	9.23×10^{8}	1.98×10^{9}	3.75×10^{9}
8	$C_6H_4H_\beta(OH)(OCH_3)$**** + 2*→ $C_6H_4H_\beta(OH)(OCH_2)$***** + H*	K_8	4.53×10^{-2}	5.02×10^{-2}	5.52×10^{-2}	6.02×10^{-2}
	ΔE_8 = 0.06 eV, $E_8^\dagger$ = 0.85 eV	k_8^+, s^{-1}	1.86×10^{3}	1.43×10^{4}	7.79×10^{4}	3.25×10^{5}
9	$C_6H_4H_\beta(OH)(OCH_3)$**** + * → C_6H_5OH**** + CH_3O*	K_9	2.53×10^{1}	2.28×10^{1}	2.11×10^{1}	1.98×10^{1}
	ΔE_9 = −0.08 eV, $E_9^\dagger$ = 1.00 eV	k_9^+, s^{-1}	2.77×10^{2}	3.24×10^{3}	2.49×10^{4}	1.39×10^{5}
10	$C_6H_4H_\alpha(OH)(OCH_3)$**** + * → $C_6H_5OCH_3$**** + OH*	K_{10}	2.01×10^{1}	1.70×10^{1}	1.49×10^{1}	1.35×10^{1}
	ΔE_{10} = −0.10 eV, $E_{10}^\dagger$ = 0.62 eV	k_{10}^+, s^{-1}	3.11×10^{7}	1.55×10^{8}	5.90×10^{8}	1.82×10^{9}
11	$C_6H_4OCH_3$**** + H* → $C_6H_5OCH_3$**** + *	K_{11}	3.47×10^{8}	4.47×10^{7}	8.16×10^{6}	1.94×10^{6}
	ΔE_{11} = −0.84 eV, $E_{11}^\dagger$ = 0.75 eV	k_{11}^+, s^{-1}	1.70×10^{5}	1.08×10^{6}	4.95×10^{6}	1.77×10^{7}
12	C_6H_4OH**** + H* → C_6H_5OH**** + *	K_{12}	5.33×10^{7}	8.64×10^{6}	1.91×10^{6}	5.33×10^{5}
	ΔE_{12} = −0.75 eV, $E_{12}^\dagger$ = 0.72 eV	k_{12}^+, s^{-1}	2.29×10^{5}	1.36×10^{6}	5.89×10^{6}	2.02×10^{7}
13	$C_6H_4(OH)(OCH_2)$***** + * → $C_6H_4(OH)$**** + CH_2O**	K_{13}	7.89×10^{-12}	1.31×10^{-10}	1.34×10^{-9}	9.47×10^{-9}
	ΔE_{13} = 1.14 eV, $E_{13}^\dagger$ = 2.23 eV	k_{13}^+, s^{-1}	2.33×10^{-10}	5.39×10^{-8}	4.86×10^{-6}	2.14×10^{-4}
14	$C_6H_4(OH)(OCH_2)$***** + * → $C_6H_4(O)(OCH_2)$***** + H*	K_{14}	1.41	1.49	1.57	1.64
	ΔE_{14} = 0.01 eV, $E_{14}^\dagger$ = 0.35 eV	k_{14}^+, s^{-1}	7.48×10^{8}	1.80×10^{9}	3.74×10^{9}	6.96×10^{9}
15	$C_6H_4(OH)(OCH_2)$***** + * → $C_6H_4(OH)(OCH)$***** + H*	K_{15}	2.44×10^{1}	1.84×10^{1}	1.47×10^{1}	1.22×10^{1}
	ΔE_{15} = −0.14 eV, $E_{15}^\dagger$ = 0.99 eV	k_{15}^+, s^{-1}	3.24×10^{2}	3.82×10^{3}	2.90×10^{4}	1.60×10^{5}
16	$C_6H_4(OH)(OCH_2)$***** → $C_6H_4(OH)(O)$**** + CH_2*	K_{16}	1.36×10^{1}	1.23×10^{1}	1.13×10^{1}	1.06×10^{1}
	ΔE_{16} = −0.07 eV, $E_{16}^\dagger$ = 0.74 eV	k_{16}^+, s^{-1}	1.61×10^{5}	1.03×10^{6}	4.79×10^{6}	1.75×10^{7}
17	$C_6H_4(OH)(O)$**** + H* → $C_6H_4(OH)_2$**** + *	K_{17}	1.27×10^{-1}	1.59×10^{-1}	1.91×10^{-1}	2.22×10^{-1}
	ΔE_{17} = 0.10 eV, $E_{17}^\dagger$ = 0.33 eV	k_{17}^+, s^{-1}	1.76×10^{9}	3.98×10^{9}	7.81×10^{9}	1.38×10^{10}
18	$C_6H_4(OH)(O)$**** + H* → $C_6H_4H_\alpha(OH)(O)$**** + *	K_{18}	3.13×10^{-10}	2.59×10^{-9}	1.47×10^{-8}	6.26×10^{-8}
	ΔE_{18} = 0.91 eV, $E_{18}^\dagger$ = 1.04 eV	k_{18}^+, s^{-1}	1.68×10^{2}	2.12×10^{3}	1.72×10^{4}	9.97×10^{4}
19	$C_6H_4(OH)(O)$**** + * → C_6H_4O**** + OH*	K_{19}	6.29×10^{-20}	5.22×10^{-18}	2.02×10^{-16}	4.38×10^{-15}
	ΔE_{19} = 1.84 eV, $E_{19}^\dagger$ = 2.35 eV	k_{19}^+, s^{-1}	2.21×10^{-12}	6.27×10^{-10}	6.71×10^{-8}	3.42×10^{-6}
20	$C_6H_4(O)(OCH_3)$**** + * → C_6H_4O**** + CH_3O*	K_{20}	3.22×10^{-14}	7.58×10^{-13}	1.03×10^{-11}	9.33×10^{-11}
	ΔE_{20} = 1.31 eV, $E_{20}^\dagger$ = 1.87 eV	k_{20}^+, s^{-1}	1.07×10^{-7}	9.52×10^{-6}	3.91×10^{-4}	8.91×10^{-3}
21	$C_6H_4(O)(OCH_3)$**** + 2* → $C_6H_4(O)(OCH_2)$***** + H*	K_{21}	2.66×10^{5}	6.75×10^{4}	2.19×10^{4}	8.58×10^{3}
	ΔE_{21} = −0.57 eV, $E_{21}^\dagger$ = 0.60 eV	k_{21}^+, s^{-1}	7.90×10^{5}	3.39×10^{6}	1.14×10^{7}	3.17×10^{7}
22	$C_6H_4H_\beta(OH)(OCH_2)$***** → $C_6H_4H_\beta(OH)(O)$**** + CH_2*	K_{22}	2.37	2.43	2.51	2.58
	ΔE_{22} = −0.02 eV, $E_{22}^\dagger$ = 0.99 eV	k_{22}^+, s^{-1}	4.92×10^{2}	5.72×10^{3}	4.38×10^{4}	2.43×10^{5}
23	$C_6H_5OCH_3$**** + * → $C_6H_5OCH_2$**** + H*	K_{23}	2.41×10^{3}	9.47×10^{2}	4.42×10^{2}	2.34×10^{2}
	ΔE_{23} = −0.39 eV, $E_{23}^\dagger$ = 0.79 eV	k_{23}^+, s^{-1}	7.76×10^{3}	5.24×10^{4}	2.56×10^{5}	9.76×10^{5}
24	$C_6H_4(OH)(OCH)$***** + * → $C_6H_4(OH)(OC)$***** + H*	K_{24}	8.25×10^{-3}	1.43×10^{-2}	2.26×10^{-2}	3.34×10^{-2}
	ΔE_{24} = 0.21 eV, $E_{24}^\dagger$ = 1.29 eV	k_{24}^+, s^{-1}	1.83×10^{-1}	4.17×10^{0}	5.55×10^{1}	4.90×10^{2}
25	$C_6H_4(OH)(OCH)$***** + * → $C_6H_4(OH)$**** + CHO**	K_{25}	9.29×10^{-3}	2.33×10^{-2}	5.02×10^{-2}	9.57×10^{-2}
	ΔE_{25} = 0.33 eV, $E_{25}^\dagger$ = 1.42 eV	k_{25}^+, s^{-1}	3.88×10^{-2}	1.30×10^{0}	2.37×10^{1}	2.73×10^{2}
26	$C_6H_4(OH)(OCH)$***** → $C_6H_4(OH)(O)$**** + CH*	K_{26}	2.18×10^{7}	4.65×10^{6}	1.31×10^{6}	4.50×10^{5}
	ΔE_{26} = −0.67 eV, $E_{26}^\dagger$ = 0.59 eV	k_{26}^+, s^{-1}	5.10×10^{6}	2.21×10^{7}	7.44×10^{7}	2.07×10^{8}
27	$C_6H_4(OH)_2$**** + * → $C_6H_4(OH)$**** + OH*	K_{27}	4.78×10^{-17}	2.06×10^{-15}	4.62×10^{-14}	6.34×10^{-13}
	ΔE_{27} = 1.57 eV, $E_{27}^\dagger$ = 2.52 eV	k_{27}^+, s^{-1}	2.46×10^{-14}	1.05×10^{-11}	1.56×10^{-9}	1.05×10^{-7}
28	$C_6H_4(OH)_2$**** + H* → $C_6H_5(OH)_2$*****	K_{28}	1.14×10^{-7}	4.77×10^{-7}	1.55×10^{-6}	4.12×10^{-6}
	ΔE_{28} = 0.64 eV, $E_{28}^\dagger$ = 1.19 eV	k_{28}^+, s^{-1}	3.89×10^{0}	6.92×10^{1}	7.45×10^{2}	5.47×10^{3}

DOI: 10.1021/cs5016244
ACS Catal. 2015, 5, 2423−2435

Table 2. continued

step	reaction	constant	T (K) 473	523	573	623
29	$C_6H_4H_\alpha(OH)(O)$**** + * → C_6H_5O**** + OH*	K_{29}	1.71	1.74	1.78	1.82
	ΔE_{29} = −0.02 eV, $E_{29}^{\dagger}$ = 1.08 eV	k_{29}^{+}, s^{-1}	3.71×10^{1}	5.18×10^{2}	4.529×10^{3}	2.88×10^{4}
30	C_6H_4O**** + H* → C_6H_5O**** + *	K_{30}	7.78×10^{9}	8.00×10^{8}	1.21×10^{8}	2.46×10^{7}
	ΔE_{30} = −0.94 eV, $E_{30}^{\dagger}$ = 0.62 eV	k_{30}^{+}, s^{-1}	3.36×10^{6}	1.56×10^{7}	5.53×10^{7}	1.60×10^{8}
31	$C_6H_4(O)(OCH_2)$***** + * → C_6H_4O**** + CH_2O*	K_{31}	5.79×10^{-14}	1.40×10^{-12}	1.95×10^{-11}	1.79×10^{-10}
	ΔE_{31} = 1.31 eV, $E_{31}^{\dagger}$ = 2.14 eV	k_{31}^{+}, s^{-1}	1.09×10^{-9}	1.97×10^{-7}	1.45×10^{-5}	5.41×10^{-4}
32	$C_6H_4(O)(OCH_2)$***** + * → $C_6H_4O_2$***** + CH_2*	K_{32}	2.60×10^{-5}	7.73×10^{-5}	1.92×10^{-4}	4.15×10^{-4}
	ΔE_{32} = 0.43 eV, $E_{32}^{\dagger}$ = 1.15 eV	k_{32}^{+}, s^{-1}	4.73×10^{0}	7.77×10^{1}	7.89×10^{2}	5.56×10^{3}
33	$C_6H_4(O)(OCH_2)$***** + * → $C_6H_4(O)(OCH)$***** + H*	K_{33}	3.58×10^{3}	1.59×10^{3}	8.19×10^{2}	4.73×10^{2}
	ΔE_{33} = −0.35 eV, $E_{33}^{\dagger}$ = 0.89 eV	k_{33}^{+}, s^{-1}	2.89×10^{3}	2.52×10^{4}	1.51×10^{5}	6.79×10^{5}
34	$C_6H_4(O)(OCH)$***** + * → $C_6H_4O_2$***** + CH*	K_{34}	2.82×10^{-1}	3.38×10^{-1}	3.96×10^{-1}	4.54×10^{-1}
	ΔE_{34} = 0.05 eV, $E_{34}^{\dagger}$ = 1.08 eV	k_{34}^{+}, s^{-1}	3.93×10^{1}	5.58×10^{2}	5.02×10^{3}	3.19×10^{4}
35	$C_6H_4(O)(OCH)$***** + * → $C_6H_4(O)(OC)$***** + H*	K_{35}	8.26×10^{-3}	1.34×10^{-2}	2.01×10^{-2}	2.84×10^{-2}
	ΔE_{35} = 0.19 eV, $E_{35}^{\dagger}$ = 1.21 eV	k_{35}^{+}, s^{-1}	8.47×10^{-1}	1.59×10^{1}	1.79×10^{2}	1.38×10^{3}
36	$C_6H_4H_\beta(OH)(O)$***** + H* → $C_6H_5(OH)_2$***** + *	K_{36}	5.31×10^{4}	1.92×10^{4}	8.26×10^{3}	4.04×10^{3}
	ΔE_{36} = −0.43 eV, $E_{36}^{\dagger}$ = 0.46 eV	k_{36}^{+}, s^{-1}	5.59×10^{7}	1.73×10^{8}	4.39×10^{8}	9.60×10^{8}
37	$C_6H_5OCH_2$**** + * → C_6H_5O**** + CH_2*	K_{37}	1.06×10^{0}	1.32×10^{0}	1.59×10^{0}	1.87×10^{0}
	ΔE_{37} = 0.06 eV, $E_{37}^{\dagger}$ = 0.93 eV	k_{37}^{+}, s^{-1}	1.44×10^{3}	1.43×10^{4}	9.55×10^{4}	4.74×10^{5}
38	C_6H_5O**** + H* → C_6H_5OH**** + *	K_{38}	6.62×10^{-1}	6.78×10^{-1}	6.89×10^{-1}	6.95×10^{-1}
	ΔE_{38} = 0.01 eV, $E_{38}^{\dagger}$ = 0.29 eV	k_{38}^{+}, s^{-1}	2.95×10^{9}	6.09×10^{9}	1.11×10^{10}	1.83×10^{10}
39	$C_6H_4(OH)(OC)$***** + * → C_6H_4OH**** + CO*	K_{39}	2.93×10^{11}	3.11×10^{10}	4.91×10^{9}	1.05×10^{9}
	ΔE_{39} = −1.01 eV, $E_{39}^{\dagger}$ = 0.63 eV	k_{39}^{+}, s^{-1}	1.89×10^{6}	9.02×10^{6}	3.29×10^{7}	9.79×10^{7}
40	$C_6H_5(OH)_2$**** + * → C_6H_5OH**** + OH*	K_{40}	2.24×10^{-2}	3.72×10^{-2}	5.71×10^{-2}	8.21×10^{-2}
	ΔE_{40} = 0.19 eV, $E_{40}^{\dagger}$ = 0.99 eV	k_{40}^{+}, s^{-1}	3.80×10^{2}	4.36×10^{3}	3.28×10^{4}	1.80×10^{5}
41	$C_6H_4O_2$***** + H* → $C_6H_4(OH)(O)$**** + 2*	K_{41}	3.72×10^{5}	1.07×10^{5}	3.77×10^{4}	1.56×10^{4}
	ΔE_{41} = −0.52 eV, $E_{41}^{\dagger}$ = 0.45 eV	k_{41}^{+}, s^{-1}	2.44×10^{8}	7.41×10^{8}	1.85×10^{9}	4.00×10^{9}
42	$C_6H_4(O)(OC)$***** → C_6H_4O**** + CO*	K_{42}	1.46×10^{7}	4.10×10^{6}	1.44×10^{6}	6.02×10^{5}
	ΔE_{42} = −0.59 eV, $E_{42}^{\dagger}$ = 0.48 eV	k_{42}^{+}, s^{-1}	1.18×10^{8}	4.01×10^{8}	1.11×10^{9}	2.62×10^{9}
43	C_6H_5OH**** + * → C_6H_5**** + OH*	K_{43}	7.44×10^{-17}	3.02×10^{-15}	6.46×10^{-14}	8.49×10^{-13}
	ΔE_{43} = 1.55 eV, $E_{43}^{\dagger}$ = 2.34 eV	k_{43}^{+}, s^{-1}	1.99×10^{-12}	5.48×10^{-10}	5.71×10^{-8}	2.84×10^{-6}
44	C_6H_5OH**** + H* → C_6H_6OH**** + *	K_{44}	5.25×10^{-7}	2.00×10^{-6}	5.97×10^{-6}	1.49×10^{-5}
	ΔE_{44} = 0.59 eV, $E_{44}^{\dagger}$ = 1.35 eV	k_{44}^{+}, s^{-1}	4.07×10^{-2}	1.03×10^{0}	1.49×10^{1}	1.40×10^{2}
45	C_6H_5**** + H* → C_6H_6*** + 2*	K_{45}	6.59×10^{7}	1.04×10^{7}	2.23×10^{6}	6.08×10^{5}
	ΔE_{45} = −0.76 eV, $E_{45}^{\dagger}$ = 0.68 eV	k_{45}^{+}, s^{-1}	1.40×10^{6}	7.73×10^{6}	3.16×10^{7}	1.03×10^{8}
46	C_6H_6OH**** → C_6H_6*** + OH*	K_{46}	9.36×10^{-3}	1.57×10^{-2}	2.41×10^{-2}	3.47×10^{-2}
	ΔE_{46} = 0.20 eV, $E_{46}^{\dagger}$ = 1.11 eV	k_{46}^{+}, s^{-1}	1.08×10^{1}	1.60×10^{2}	1.50×10^{3}	9.87×10^{3}
47	CH* + H* → CH_2* + *	K_{47}	2.77×10^{-8}	1.54×10^{-7}	6.29×10^{-7}	2.04×10^{-6}
	ΔE_{47} = 0.73 eV, $E_{47}^{\dagger}$ = 0.80 eV	k_{47}^{+}, s^{-1}	2.67×10^{4}	1.86×10^{5}	9.22×10^{5}	3.53×10^{6}
48	CH_2* + H* → CH_3* + *	K_{48}	7.89	7.91	7.86	7.78
	ΔE_{48} = −0.01 eV, $E_{48}^{\dagger}$ = 0.62 eV	k_{48}^{+}, s^{-1}	3.21×10^{6}	1.48×10^{7}	5.20×10^{7}	1.49×10^{8}
49	CH_3* + H* → CH_4* + *	K_{49}	8.07×10^{-2}	1.58×10^{-1}	2.73×10^{-1}	4.31×10^{-1}
	ΔE_{49} = 0.24 eV, $E_{49}^{\dagger}$ = 0.77 eV	k_{49}^{+}, s^{-1}	6.71×10^{4}	4.46×10^{5}	2.13×10^{6}	7.91×10^{6}
50	CHO** + H* → CH_2O** + *	K_{50}	3.49×10^{-11}	3.05×10^{-10}	1.82×10^{-9}	8.10×10^{-9}
	ΔE_{50} = 0.95 eV, $E_{50}^{\dagger}$ = 1.25 eV	k_{50}^{+}, s^{-1}	2.19×10^{-1}	4.28×10^{0}	4.95×10^{1}	3.87×10^{2}
51	CH_2O** + H* → CH_3O* + 2*	K_{51}	2.09×10^{-6}	8.03×10^{-6}	2.42×10^{-5}	6.06×10^{-6}
	ΔE_{51} = 0.57 eV, $E_{51}^{\dagger}$ = 0.61 eV	k_{51}^{+}, s^{-1}	4.04×10^{6}	1.79×10^{7}	6.13×10^{7}	1.72×10^{8}
52	CH_3O* + H* → CH_3OH* + *	K_{52}	1.78×10^{4}	7.66×10^{3}	3.80×10^{3}	2.10×10^{3}
	ΔE_{52} = −0.36 eV, $E_{52}^{\dagger}$ = 0.31 eV	k_{52}^{+}, s^{-1}	2.80×10^{9}	6.14×10^{9}	1.17×10^{10}	2.02×10^{10}
53	OH* + H* → H_2O* + *	K_{53}	6.67×10^{6}	1.97×10^{6}	7.16×10^{5}	3.06×10^{5}
	ΔE_{53} = −0.55 eV, $E_{53}^{\dagger}$ = 0.20 eV	k_{53}^{+}, s^{-1}	7.89×10^{10}	1.35×10^{11}	2.10×10^{11}	3.04×10^{11}
54	$C_6H_5OCH_3$**** → $C_6H_5OCH_3$(gas) + 4*	K_{54}	6.13×10^{-9}	5.03×10^{-6}	1.57×10^{-3}	2.33×10^{-1}
	ΔE_{54} = 2.31 eV	k_{54}^{+}, s^{-1}	4.77×10^{-1}	3.73×10^{2}	1.11×10^{5}	1.58×10^{7}
55	$C_6H_4(OH)_2$**** → $C_6H_4(OH)_2$(gas) + 4*	K_{55}	5.00×10^{-10}	4.74×10^{-7}	1.64×10^{-4}	2.64×10^{-2}
	ΔE_{55} = 2.39 eV	k_{55}^{+}, s^{-1}	3.86×10^{-2}	3.48×10^{1}	1.15×10^{4}	1.77×10^{6}
56	C_6H_5OH**** → C_6H_5OH(gas) + 4*	K_{56}	1.58×10^{-9}	9.00×10^{-7}	1.98×10^{-4}	2.17×10^{-2}
	ΔE_{56} = 2.24 eV	k_{56}^{+}, s^{-1}	1.32×10^{-1}	7.14×10^{1}	1.50×10^{4}	1.58×10^{6}
57	C_6H_6*** → C_6H_6(gas) + 3*	K_{57}	2.17×10^{-10}	8.10×10^{-8}	1.25×10^{-5}	9.38×10^{-4}
	ΔE_{57} = 2.14 eV	k_{57}^{+}, s^{-1}	1.99×10^{-2}	7.06×10^{0}	1.04×10^{3}	7.77×10^{4}
58	CH_4* → CH_4(gas) + *	K_{58}	3.29×10^{6}	9.50×10^{6}	2.37×10^{7}	5.41×10^{7}

DOI: 10.1021/cs5016244
ACS Catal. 2015, 5, 2423−2435

Table 2. continued

step	reaction	constant	T (K) 473	523	573	623
	ΔE_{58} = 0.26 eV	k_{58}^{+}, s^{-1}	6.65×10^{14}	1.83×10^{15}	4.36×10^{15}	9.54×10^{15}
59	$CH_3OH^* \rightarrow CH_3OH(gas) + *$	K_{59}	6.26×10^{4}	4.63×10^{5}	2.63×10^{6}	1.18×10^{7}
	ΔE_{59} = 0.63 eV	k_{59}^{+}, s^{-1}	8.95×10^{12}	6.30×10^{13}	3.41×10^{14}	1.47×10^{15}
60	$H_2O^* \rightarrow H_2O(gas) + *$	K_{60}	5.02×10^{4}	1.91×10^{5}	5.98×10^{5}	1.62×10^{6}
	ΔE_{60} = 0.40 eV	k_{60}^{+}, s^{-1}	9.57×10^{12}	3.46×10^{13}	1.04×10^{14}	2.70×10^{14}
61	$CO^* \rightarrow CO(gas) + *$	K_{61}	2.67×10^{-13}	4.55×10^{-11}	3.29×10^{-9}	1.25×10^{-7}
	ΔE_{61} = 2.02 eV	k_{61}^{+}, s^{-1}	4.08×10^{-5}	6.61×10^{-3}	4.57×10^{-1}	1.66×10^{1}
62	$H^* \rightarrow 0.5H_2(gas) + *$	K_{62}	1.95×10^{-3}	8.18×10^{-2}	2.71×10^{-2}	7.50×10^{-2}
	ΔE_{62} = 0.54 eV	k_{62}^{+}, s^{-1}	1.50×10^{6}	5.96×10^{6}	1.89×10^{7}	5.01×10^{7}

group of guaiacol to C_6H_4OH (step 4) (ΔE_0 = 1.22 eV) is similarly difficult, with an activation barrier of 2.14 eV. Again, subsequent hydrogenation to phenol (step 12) (ΔE_0 = −0.75 eV) is kinetically possible, with a barrier of 0.72 eV. Finally, in pathway 6, the direct removal of the methyl group of guaiacol to form $C_6H_4(OH)(O)$ (step 6) (ΔE_0 = −0.58 eV) is prohibitive, with a barrier of 2.00 eV. Subsequent thermoneutral (ΔE_0 = 0.10 eV) hydrogenation of $C_6H_4(OH)(O)$ to catechol (step 17) is again facile, with a low barrier of only 0.33 eV.

3.3.3. Reaction Pathways with Initial Dehydrogenation of a Functional Group. In this section, we investigate if dehydrogenation of the $-OCH_3$ (pathway 5) or the −OH (pathway 7) group can activate guaiacol to permit a more facile deoxygenation. In the fifth pathway, the methoxy group of guaiacol is dehydrogenated to produce $C_6H_4(OH)(OCH_2)$ (step 5). This exothermic step (ΔE_0 = −0.50 eV) is facile, with an activation barrier of 0.71 eV. $C_6H_4(OH)(OCH_2)$ can undergo four possible reaction pathways. Removal of the $-OCH_2$ group (step 13) is highly endothermic (ΔE_0 = 1.14 eV) and possesses a high activation barrier of 2.23 eV. Further dehydrogenation of the $-OCH_2$ group (step 15) is slightly exothermic (ΔE_0 = −0.14 eV), but also involves overcoming a significant activation barrier of 0.99 eV. In contrast, the thermoneutral dehydrogenation of the −OH group (step 14) and methylene removal to form $C_6H_4(OH)(O)$ (step 16) possess activation barriers of only 0.35 and 0.74 eV, respectively. Reaction steps of the product of step 14, $C_6H_4(O)(OCH_2)$, will be further discussed in the context of the seventh pathway. $C_6H_4(OH)(O)$ can be hydrogenated to catechol, which is facile (see above), or to $C_6H_4H_\alpha(OH)(O)$ (step 18) to activate the phenyl ring. The activation of the phenyl ring is a highly endothermic process (ΔE_0 = 0.91 eV) with a significant barrier of 1.04 eV. However, dehydroxylation of $C_6H_4H_\alpha(OH)(O)$ to phenoxy (step 29) is thermoneutral and involves overcoming an activation barrier of only 0.68 eV. As discussed above, phenoxy can easily be hydrogenated to phenol (step 38). Alternatively, $C_6H_4(OH)(O)$ can be dehydroxylated to C_6H_4O (step 19), but on Pt, this constitutes a highly endothermic process (ΔE_0 = 1.84 eV) with a high barrier of 2.35 eV. Similarly, catechol cannot dehydroxylate to C_6H_4OH (step 27) (ΔE_0 = 1.84 eV, E_a = 2.52 eV). To deoxygenate catechol, the phenyl ring has to be hydrogenated to $C_6H_5(OH)_2$ (step 28), which is similar to all activations of the phenyl ring, an endothermic process (ΔE_0 = 0.64 eV) with an activation barrier of over 1 eV (E_a = 1.19 eV). Then dehydroxylation to phenol (step 40) is potentially feasible at higher temperatures (ΔE_0 = 0.19 eV, E_a = 0.99 eV).

In the seventh reaction pathway, guaiacol is activated by initial dehydrogenation of the −OH group (step 7) to produce $C_6H_4(O)(OCH_3)$. This slightly endothermic process (ΔE_0 = 0.08 eV) possesses a very low activation barrier of only 0.37 eV. Next, the $C_6H_4(O)(OCH_3)$ species can decompose by methoxy removal (step 20), which is quite challenging (ΔE_0 = 1.31 eV, E_a = 1.87 eV) and occurs more likely by further dehydrogenation (step 21) to produce $C_6H_4(O)(OCH_2)$ (ΔE_0 = −0.57 eV, E_a = 0.60 eV). $C_6H_4(O)(OCH_2)$ can also be produced by the fifth reaction pathway, and both pathways merge at this species (or the hydrogenated counterpart $C_6H_4(OH)(OCH_2)$; see above). Removal of the $-OCH_2$ group from $C_6H_4(O)(OCH_2)$ (step 31) is a highly endothermic process (ΔE_0 = 1.31 eV) with a high activation barrier of 2.14 eV. Instead, the $C_6H_4(O)(OCH_2)$ species can dehydrogenate to $C_6H_4(O)(OCH)$ (step 33: ΔE_0 = −0.35 eV, E_a = 0.89 eV) or remove its methylene group to $C_6H_4(O)_2$ (step 32: ΔE_0 = 0.43 eV, E_a = 1.15 eV). $C_6H_4(O)_2$ can easily be hydrogenated to catechol. Next, $C_6H_4(O)(OCH)$ can react on the Pt surface by dehydrogenation to $C_6H_4(O)(OC)$ (step 35: ΔE_0 = 0.19 eV, E_a = 1.21 eV) or by −CH removal to $C_6H_4(O)_2$ (step 34: ΔE_0 = 0.05 eV, E_a = 1.08 eV). Finally, $C_6H_4(O)(OC)$ can decarbonylate to $C_6H_4(O)$, which is facile (step 42: ΔE_0 = −0.59 eV, E_a = 0.48 eV). In addition, the hydrogenation of $C_6H_4(O)$ to phenoxy (step 30: ΔE_0 = −0.94 eV, E_a = 0.62 eV) and phenol (step 12: ΔE_0 = −0.75 eV, E_a = 0.72 eV) are facile.

Overall, in pathway 7, the lowest-energy pathway to produce catechol involves production of $C_6H_4(O)(OCH_2)$ and its hydrogenated counterpart $C_6H_4(OH)(OCH_2)$, followed by methylene removal and hydrogenation, as in pathway 5. To produce phenol, the highest barrier in pathway 7 is the last dehydrogenation of the methoxy group, followed by facile decarbonylation (E_a = 1.21 eV). It is interesting to note that the dehydrogenation of the phenolic alcohol group did not substantially change the kinetics of processes on the neighboring methoxy group; compare, for example, step 13 ($C_6H_4(OH)(OCH_2) \rightarrow C_6H_4(OH) + CH_2O$; ΔE_0 = 1.14 eV, E_a = 2.23 eV) and step 31 ($C_6H_4(O)(OCH_2) \rightarrow C_6H_4(O) + CH_2O$; ΔE_0 = 1.31 eV, E_a = 2.14 eV) or step 5 ($C_6H_4(OH)(OCH_3) \rightarrow C_6H_4(OH)(OCH_2) + H$; ΔE_0 = −0.50 eV, E_a = 0.71 eV) and step 21 ($C_6H_4(O)(OCH_3) \rightarrow C_6H_4(O)(OCH_2) + H$; ΔE_0 = −0.57 eV, E_a = 0.60 eV). Next, we can conclude that Pt catalysts can quite easily convert guaiacol to catechol: $C_6H_4(OH)(OCH_3) \rightarrow C_6H_4(OH)(OCH_2) \rightarrow C_6H_4(OH)(O) \rightarrow C_6H_4(OH)_2$; however, deoxygenation of guaiacol by decarbonylation, direct phenyl−OH bond cleavage, or activation of the phenyl ring by hydrogenation is slow.

DOI: 10.1021/cs5016244
ACS Catal. 2015, 5, 2423−2435

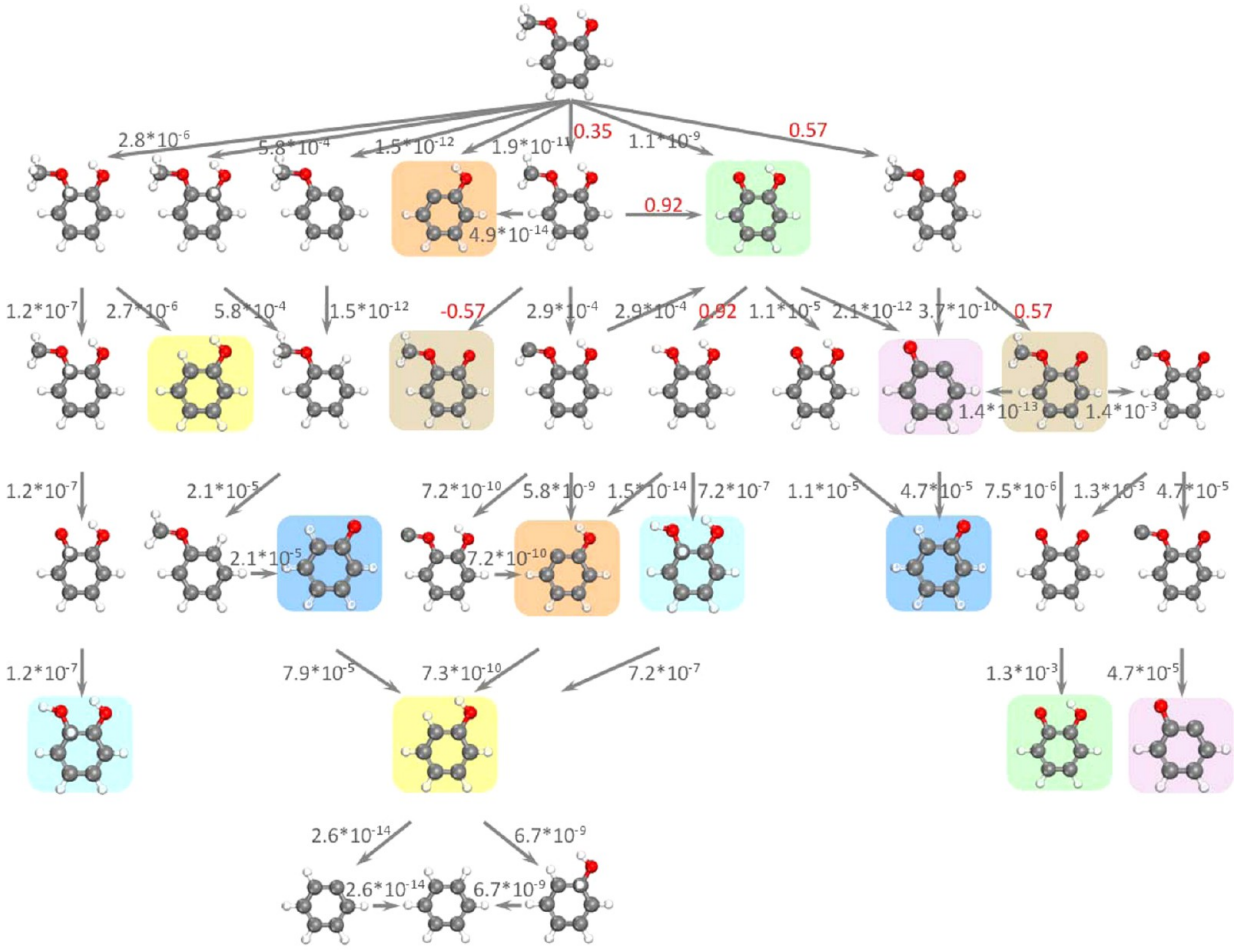

Figure 4. Turnover frequencies (s^{-1}) of all elementary steps at a temperature of 573 K and reactant pressures of guaiacol and hydrogen of 1 bar. For clarity, duplicate structures are highlighted by identical background colors.

3.3.4. Deoxygenation Steps by Direct Phenyl(C)-O Bond Dissociation. The discussion above and our microkinetic model described below do not include deoxygenation steps by direct phenyl(C)-O bond scissions because we consistently find that these steps have very high reaction barriers over Pt(111). For instance, O removal of $C_6H_4(O)(OCH_3)$, $C_6H_4O_2$, and C_6H_5O needs to overcome a barrier of 2.79, 3.06, and 3.09 eV, respectively.

3.4. Turnover Frequencies from Microkinetic Modeling. Analysis of the elementary reaction energies without building a microkinetic model and considering temperature and partial pressures is often difficult such that we decided to develop a mean-field microkinetic model that considers lateral interactions among key surface intermediates approximately using a method similar to the one proposed by Grabow et al.[36] We note that other functional forms for describing lateral interactions have been proposed and that we selected the method from Grabow et al. primarily for its simplicity and ability to fit our DFT data.

Preliminary results of our microkinetic model showed that H and CO are the two most abundant surface intermediates. From adsorption energy calculations of H on Pt(111) at various coverages (θ_H = 1/4, 2/4, 3/4, and 4/4 ML), we determined a differential adsorption energy of H for the reaction $0.5H_{2(gas)} + * \rightarrow H^*$ as a function of θ_H and $E_H(\theta_H)$, as shown in eq 2.

$$E_H(\theta_H) = -0.537 + 2 \times 0.094 \times (\theta_H - 0.183) \quad (2)$$

Similarly, from adsorption energy calculations of CO at various coverages (θ_{CO} = 1/4, 2/, 3/4, and 4/4 ML), we determined a differential adsorption energy of phenoxy as a function of θ_{CO}, $E_{CO}(\theta_{CO})$, as shown in eq 3.

$$E_{CO}(\theta_{CO}) = -2.020 + 2 \times 1.374 \times (\theta_H - 0.117) \quad (3)$$

Finally, coadsorption of H and CO at various coverages leads to $E_H(\theta_H, \theta_{CO})$ and $E_{CO}(\theta_H, \theta_{CO})$ in eqs 4 and 5, respectively.

$$E_H(\theta_H, \theta_{CO}) = -0.537 + 2 \times 0.094 \times (\theta_H - 0.183) + 0.526\theta_{CO} + 1.5 \times 0.075 \times \theta_{CO}(\theta_H\theta_{CO})^{0.5} \quad (4)$$

$$E_{CO}(\theta_H, \theta_{CO}) = -2.020 + 2 \times 1.374 \times (\theta_H - 0.117) + 0.526\theta_H + 1.5 \times 0.075 \times \theta_H(\theta_H\theta_{CO})^{0.5} \quad (5)$$

Considering that the aim of our microkinetic model is not to simulate experimental observations but only to understand the reaction mechanism under characteristic reaction conditions, the partial pressures of the reactants, guaiacol, and H_2 were fixed to 1 bar, and the partial pressures of possible reaction products (anisole, catechol, phenol, benzene, CO, CH_4, CH_3OH, and H_2O) were fixed to 0.01 bar (~1% conversion).

DOI: 10.1021/cs5016244
ACS Catal. 2015, 5, 2423−2435

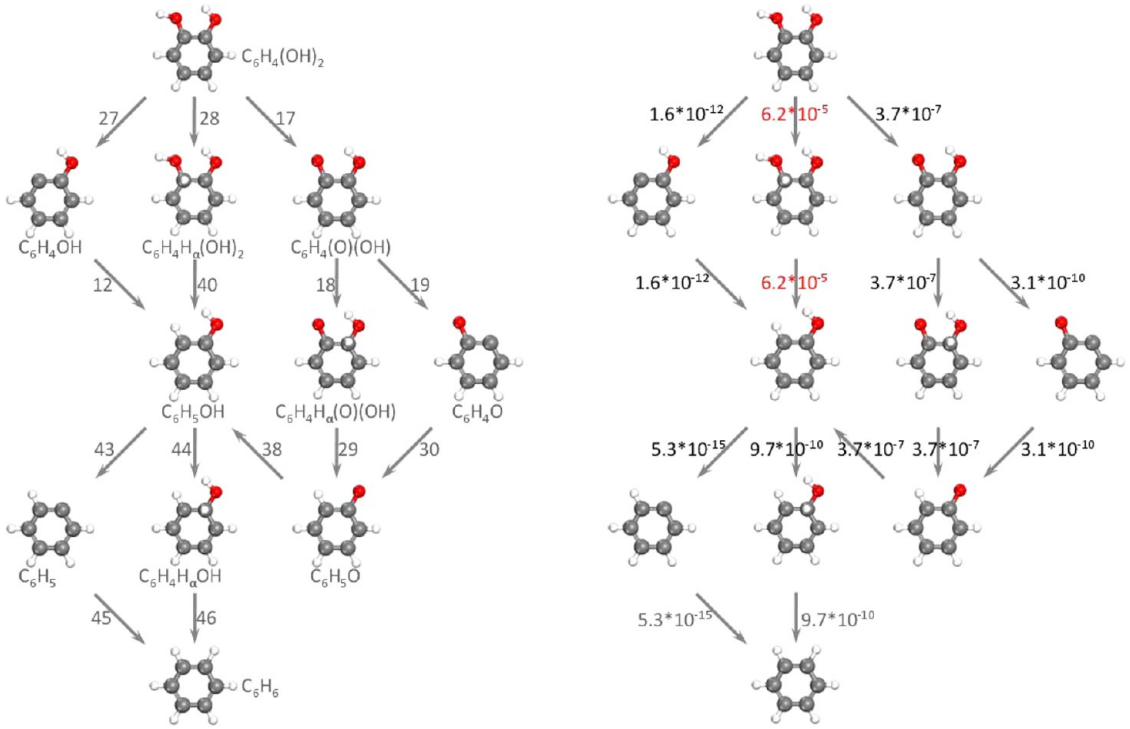

Figure 5. Turnover frequencies (s^{-1}) of the HDO of catechol (1 bar) in a reaction environment of 1 bar of H_2 and 10^{-2} bar of CO at 573 K.

The reaction temperature was fixed to 573 K, which is a characteristic experimental temperature for the HDO over Pt catalysts. In the Supporting Information, we show that at 573 K, the hydrogenation of the phenyl ring, for example, the hydrogenation of benzene, phenol, and catechol to cyclohexane, cyclohexanol, and 1,2-cyclohexanediol, respectively, is thermodynamically limited. Under these conditions, we find that the CH, H, CO, and free site coverages are 54.1%, 8.8%, 31.4% and 5.3%, respectively. Other surface intermediates, including all aromatic surface intermediates, do not have any noticeable surface coverage. We note that the predicted CO coverage is likely too large because the PBE-D3 functional overestimates the CO adsorption energy. However, considering that adsorbed CO poisons essentially only the Pt(111) surface in our model and that the free site coverage is reasonably large (5.3%), we do not expect the accuracy of the DFT functional to significantly affect our mechanistic predictions. Next, the turnover frequencies of all elementary steps in the reaction network are shown in Figure 4.

The microkinetic model suggests that HDO pathways involving hydrogenations of the phenyl ring are unfavorable. Pathways starting with hydrogenations of the aromatic ring are slow with TOFs of 2.8×10^{-6} s^{-1} for pathway 1 and 5.8×10^{-4} s^{-1} for pathway 2, respectively. The model also shows that pathways starting with direct removal of the −OH (pathway 3), $-OCH_3$ (pathway 4), and $-CH_3$ groups (pathway 6) are prohibitively slow with TOFs of 1.5×10^{-12} s^{-1}, 1.9×10^{-11} s^{-1}, and 1.1×10^{-9} s^{-1}, respectively.

Instead, the model suggests that pathways starting with dehydrogenation steps of functional groups are favored. Pathway 5 starting with $-OCH_3$ dehydrogenation of guaiacol has a TOF of 0.35 s^{-1}, and pathway 7 starting with −OH dehydrogenation of guaiacol followed by $-OCH_3$ dehydrogenation has a TOF of 0.57 s^{-1}. Ultimately, both pathways 5 and 7 merge at the dehydrogenated methoxy group species, $C_6H_4(OH)(OCH_2)$, from which the methylene group is removed to produce $C_6H_4(OH)(O)$ and which can easily be hydrogenated to catechol. We note that conversion of guaiacol to catechol is not a deoxygenation process and that the deoxygenation of catechol by hydrogenation of the phenyl ring (steps 28 and 40) or by decarbonylation of guaiacol (steps 42, 25, 39) is ∼4 orders of magnitude slower than the conversion of guaiacol to catechol.

Production of phenol can occur by three pathways. One is the α-carbon hydrogenation of guaiacol to $C_6H_4H_\alpha(OH)(OCH_3)$ (step 2), followed by its dehydroxylation to $C_6H_5OCH_3$ (anisole) and anisole dehydrogenation to $C_6H_5OCH_2$, followed by methylene removal to C_6H_5O, which is finally hydrogenated to phenol with a TOF of 2.1×10^{-5} s^{-1}. The second one is dehydrogenation of guaiacol to $C_6H_4(O)(OC)$, followed by decarbonylation to C_6H_4O and hydrogenation to phenol with a TOF of 4.7×10^{-5} s^{-1}. The third one is the methyl group removal of guaiacol to $C_6H_4(OH)(O)$, followed by hydrogenation of the phenyl ring to $C_6H_4H_\alpha(OH)(O)$ (step 18), dehydroxylation to C_6H_5O, and hydrogenation to phenol with a TOF of 1.1×10^{-5} s^{-1}. The overall TOF of phenol production is 7.9×10^{-5} s^{-1}, which is still 4 orders of magnitude lower than catechol production. Considering the low phenol production rate, deoxygenation of phenol to benzene, occurring primarily by hydrogenation of the phenyl ring (step 46), is also slow, with a TOF of 6.7×10^{-9} s^{-1}, that is, 4 orders of magnitude slower than phenol production.

Given that the production rate of catechol is significant, we investigated if once produced catechol can be deoxygenated to phenol. Figure 5 illustrates the hydrodeoxygenation pathways of catechol. Assuming a reaction temperature of 573 K and partial pressures of catechol, H_2, CO, phenol, benzene, and water of 1, 1, 10^{-2}, 10^{-2}, 10^{-2}, and 10^{-2} bar, respectively, the surface intermediates with significant coverages are CO

DOI: 10.1021/cs5016244
ACS Catal. 2015, 5, 2423−2435

(31.6%), $C_6H_4(O)(OH)$ (49.2%), H (4.4%), free sites (3.8%), and catechol (11.2%). The dominant HDO pathway proceeds by hydrogenation of catechol to $C_6H_4H_\alpha(OH)_2$ (step 28), followed by dehydroxylation of the α-carbon to phenol with a TOF of 6.2×10^{-5} s^{-1}. We note here again that we assumed in our microkinetic models that the isomerization of the hydrogenated catechol structure with H atom close to the Pt(111) surface (the structure formed during hydrogenation) and the corresponding structure with the −OH group close to Pt(111) (the structure from which the C−OH bond scission can occur) is rapid. If, indeed, no such pathway exists for this isomerization reaction, then Pt(111) cannot deoxygenate catechol to phenol or benzene at 573 K (the TOF would be reduced to $\sim 3.1 \times 10^{-10}$ s^{-1}).

We conclude that over Pt(111), deoxygenation of guaiacol occurs by decarbonylation or possibly by formation of catechol and hydrogenation of the phenyl ring. Both pathways are 4 orders of magnitude slower than formation of catechol. If our assumption of a fast isomerization step (discussed above) is not valid, slow deoxygenation of guaiacol over Pt(111) occurs exclusively by decarbonylation. Considering that hydrogenation of the phenyl ring is also the initial step for production of cycloalkanes at lower temperatures where hydrogenation of the phenyl ring is thermodynamically favorable (see Supporting Information), it will be challenging to design low-temperature Pt-based catalysts with a high selectivity to aromatic products. Instead, we recommend for a low-temperature process more oxophilic transition metals that are able to decarbonylate the methoxy group of guaiacol more efficiently or can directly split the phenyl(C)−OH bond. In fact, Chiu et al.[37] and Lu and Heyden[38] recently showed by DFT calculations that Ru(0001) is active for direct C−OH bond cleavage and decarbonylation, although the predicted turnover frequency for the conversion of guaiacol over Ru(0001) is lower than the guaiacol conversion to catechol predicted here.[38]

Overall, our computational predictions agree only partially with experimental observations under various hydrogenation conditions. Gutierrez et al.[9] have studied the hydrodeoxygenation of guaiacol over Pt/ZrO_2 at 373 K and 80 bar of H_2 for 5 h and found the main products are cyclohexanol, 1-methyl-1,2-cyclohexanediol, and 1,2-dimethoxy-benzene, that is, diols are formed, and if deoxygenation occurs, the phenyl ring is hydrogenated at high H_2 partial pressures and low temperatures. The observed hydrogenation of the phenyl at this low temperature can be understood by our DFT study that finds hydrogenation barriers of the phenyl ring that are only slightly larger than 1 eV. In contrast, the (although limited) degree of deoxygenation observed cannot be rationalized with our calculations on Pt(111). We expect that Pt step sites or the oxide support are responsible for the observed deoxygenation.

Next, Nimmanwudipong et al.[13] have studied the hydrogenation of guaiacol over Pt/Al_2O_3 at 573 K and 0.42 bar of H_2 and found that the main reaction products are catechol (41.2%), phenol (31.6%), and 3-methyl-catechol (12.5%). The production of catechol as the main reaction product can be rationalized from our calculations, while again the phenol production cannot be explained by Pt(111) sites. Finally, Sun et al.[5] have investigated the guaiacol hydrodeoxygenation over Pt/C at 523 and 623 K and low H_2 partial pressures of 0.4 bar. At the lower temperature, they observed primarily phenol (∼50%), cyclohexanone (∼10%), and cyclohexanol (∼5%) as major reaction products, whereas at higher temperatures they observed primarily phenol (30%) and benzene (30%). Although we understand the hydrogenation of the phenyl ring at lower temperatures, we cannot explain the absence of significant amounts of catechol in their reaction product. It seems to us that the carbon support or less-coordinated Pt step and corner sites are responsible for the observed higher HDO activity.[18]

3.5. Sensitivity Analysis. *3.5.1. Degree of Rate Control.* We have used Campbell's degree of rate control,[39−42] X_{RC}, to determine the rate-controlling steps in the mechanism. The degree of rate control is defined as

$$X_{RC,i} = \frac{k_i}{r}\left(\frac{\partial r}{\partial k_i}\right)_{K_i, k_j \neq k_i} \tag{6}$$

where r is the overall rate of reaction. Rate-controlling steps are identified by nonzero X_{RC} values. In the following, we report only rate-control values that deviate from zero. Under the reaction conditions mentioned above for the hydrogenation of guaiacol, we found a degree of rate control of 0.38 for the CH_2 hydrogenation to CH_3 (step 48) and 0.61 for the CH_3 hydrogenation to CH_4 (step 49). Both steps are related to the removal of surface CH species, which we find to have a significant surface coverage. If we artificially increase the reaction rates for these two steps, we observe that the dehydrogenation steps of the methoxy group (step 5 and 21) are the most rate-controlling. Next, for the hydrodeoxygenation of catechol, we find the dehydroxylation of $C_6H_4H_\alpha(OH)_2$ to C_6H_5OH (step 40) to be the sole rate-controlling step, $X_{RC} = 1$.

3.5.2. Degree of Thermodynamic Rate Control. The degree of thermodynamic rate control,[41−43] X_{TRC}, is used to analyze the sensitivity of the microkinetic model with regards to the binding energy of the surface intermediates:

$$X_{TRC,n} = \frac{1}{r}\left(\frac{\partial r}{\partial\left(\frac{-G_n^0}{RT}\right)}\right)_{G_{m\neq n}^0, G_i^{0,TS}} \tag{7}$$

where r is the overall rate of reaction and G_n^0 is the free energy of adsorbate n. Rate-controlling intermediates are identified by nonzero X_{TRC} values. In the following, we report only thermodynamic rate-control values that deviate from zero. Negative values signify that reducing the adsorption strength will increase the rate, and positive values signify that increasing the adsorption strength will increase the reaction rate. Under the reaction conditions mentioned above for the hydrogenation of guaiacol, the adsorbed CH and CO have a degree of thermodynamic rate control of −0.99 and −0.42, respectively, illustrating the poisoning effect of these species. Next, H has an X_{TRC} of 2.00, suggesting that stronger H binding would facilitate conversion by increasing the CH removal rate. Next, for the hydrodeoxygenation of catechol, we find a negative X_{TRC} for catechol ($X_{TRC} = -1.74$), and CO ($X_{TRC} = -0.40$), symbolizing an inhibiting effect and positive X_{TRC} values for hydrogen ($X_{TRC} = 1.98$) and $C_6H_4(O)(OH)$ ($X_{TRC} = 0.96$) which an idealized catalyst should adsorb more strongly.

3.6. Apparent Activation Energy and Reaction Orders. Finally, we calculated for our model the apparent activation energy (E_a) in the temperature range of 523−623 K and the reaction orders (α_i) of guaiacol, H_2, and CO at 573 K in the guaiacol model to better understand the sensitivity of our results to changes in temperature and partial pressure.

DOI: 10.1021/cs5016244
ACS Catal. 2015, 5, 2423−2435

$$E_a = RT^2\left(\frac{\partial \ln(r)}{\partial T}\right)_{P,p_i} \quad (8)$$

$$\alpha_i = \left(\frac{\partial \ln(r)}{\partial \ln(p_i)}\right)_{T,P} \quad (9)$$

Our model predicts an apparent activation barrier of 1.21 eV (116 kJ/mol). As for the reaction orders, our model predicts a guaiacol order of 0.04 in the pressure range of 0.01−1.0 bar, a H_2 order of 1.0 in the range of 0.1−10 bar, and a CO order of −0.44 in the range of 0.005−0.1 bar. Clearly, a higher H_2 partial pressure is desirable for the conversion of guaiacol. However, considering that a higher H_2 partial pressure will also lead to a more extensive hydrogenation of the phenyl ring at lower temperatures, the H_2 partial pressure can be increased only if the reaction temperature is above 523−573 K, where hydrogenation of the phenyl ring is thermodynamically limited.

For the hydrodeoxygenation of catechol, we find a high apparent activation barrier of 2.63 eV (253 kJ/mol) in the temperature range of 523−623 K, a catechol order of −0.14 in the range of 0.1−10 bar, a H_2 order of 0.99 in the range of 0.1−5 bar, and a CO order of −0.40 in the range of 10^{-4}−10^{-1} bar.

4. CONCLUSIONS

A microkinetic model based on parameters obtained from density functional theory calculations and transition state theory has been developed to investigate the hydrodeoxygenation mechanism of guaiacol over a Pt(111) model surface at a temperature of 573 K, where the hydrogenation of the phenyl ring is thermodynamically limited. The microkinetic model identified two hydrogenation pathways leading to catechol. One pathway proceeds via $-OCH_3$ dehydrogenation of guaiacol, $[C_6H_4(OH)(OCH_3)]$, to yield $C_6H_4(OH)(OCH_2)$ followed by $-CH_2$ removal to $C_6H_4(OH)(O)$ and then hydrogenation of $C_6H_4(OH)(O)$ to catechol $[C_6H_4(OH)_2]$. The other pathway proceeds via −OH dehydrogenation of guaiacol to $C_6H_4(O)(OCH_3)$, then $-OCH_3$ dehydrogenation of $C_6H_4(O)(OCH_3)$ to $C_6H_4(O)(OCH_2)$ and eventually hydrogenation to $C_6H_4(OH)(OCH_2)$ followed, as before, by $-CH_2$ removal to $C_6H_4(OH)(O)$ and then hydrogenation of $C_6H_4(OH)(O)$ to catechol. Catechol is found to be the major reaction product, and deoxygenation to phenol or benzene is found to be ∼4 orders of magnitude slower than production of catechol. The preferred deoxygenation pathway on Pt(111) proceeds by decarbonylation and possibly partial hydrogenation of the phenyl ring to $C_6H_4H_\alpha(OH)_2$, followed by −OH removal and phenol production. Reaction pathways that involve direct −OH removal without activation of the phenyl ring are found to be at least 5 orders of magnitude slower. The rate-controlling deoxygenation step of catechol is the −OH removal. The reaction order of H_2 is ∼1 for the deoxygenation of guaiacol and catechol, suggesting that a higher hydrogen pressure would facilitate deoxygenation. However, considering that a higher hydrogen pressure can also lead to a hydrogenation of the phenyl ring and production of cycloalkanes, this strategy can be applied only at temperatures above 523−573 K, where hydrogenation of the phenyl ring is thermodynamically limited. Overall, this computational study significantly disagrees with some experimental observations that suggest Pt catalysts can deoxygenate guaiacol and catechol. We rationalize this experimental observation by active involvement of the catalyst support or Pt step or corner sites in the deoxygenation process. Our study suggests that Pt(111) sites are not active deoxygenation sites.

■ ASSOCIATED CONTENT

Supporting Information

The following file is available free of charge on the ACS Publications website at DOI: 10.1021/cs5016244.

Pathways for C−OH bond cleavage in catechol by hydrogenation of the phenyl ring, thermodynamic information for the hydrogenation of phenyl rings, structures of various small reaction intermediates and transition states (PDF)

■ AUTHOR INFORMATION

Corresponding Author

*Phone: +1-803-777-5025. Email: heyden@cec.sc.edu.

Notes

The authors declare no competing financial interest.

■ ACKNOWLEDGMENTS

We acknowledge Dr. Aravind Asthagiri from The Ohio State University for helping us obtain and install the VASP D3 corrections for dispersion interactions. This work has been supported by the U.S. Department of Energy, Office of Basic Energy Sciences, Chemical Sciences Division under Contract DE-FG02-11ER16268 (DE-SC0007167). Computational resources have been provided by the National Energy Research Scientific Computing Center (NERSC), which is supported by the Office of Science of the U.S. Department of Energy and in part by TeraGrid under Grant No. TG-CTS090100. Finally, computing resources from USC's High Performance Computing Group are gratefully acknowledged.

■ REFERENCES

(1) Xiu, S.; Shahbazi, A. *Renew., Sust. Energy Rev.* **2012**, *16*, 4406−4414.

(2) Oasmaa, A.; Kuoppala, E.; Ardiyanti, A.; Venderbosch, R. H.; Heeres, H. J. *Energy Fuels* **2010**, *24*, 5264−5272.

(3) Sfetsas, T.; Michailof, C.; Lappas, A.; Li, Q.; Kneale, B. *J. Chromatogr. A* **2011**, *1218*, 3317−3325.

(4) Olcese, R. N.; Bettahar, M.; Petitjean, D.; Malaman, B.; Giovanella, F.; Dufour, A. *Appl. Catal., B* **2012**, *115−116*, 63−73.

(5) Sun, J. M.; Karim, A. M.; Zhang, H.; Kovarik, L.; Li, X. S.; Hensley, A. J.; McEwen, J.-S.; Wang, Y. *J. Catal.* **2013**, *306*, 47−57.

(6) Chang, J.; Danuthai, T.; Dewiyanti, S.; Wang, C.; Borgna, A. *ChemCatChem* **2013**, *5*, 3041−3049.

(7) Elliott, D. C.; Hart, T. R. *Energy Fuels* **2009**, *23*, 631−637.

(8) Zhao, C.; He, J.; Lemonidou, A. A.; Li, X.; Lercher, J. A. *J. Catal.* **2011**, *280*, 8−16.

(9) Gutierrez, A.; Kaila, R. K.; Honkela, M. L.; Slioor, R.; Krause, A. O. I. *Catal. Today* **2009**, *147*, 239−246.

(10) Lin, Y.; Li, C.; Wan, H.; Lee, H.; Liu, C. *Energy Fuels* **2011**, *25*, 890−896.

(11) Gao, D.; Schweitzer, C.; Hwang, H. T.; Varma, A. *Ind. Eng. Chem. Res.* **2014**, *53*, 18658−18667.

(12) Nimmanwudipong, T.; Aydin, C.; Lu, J.; Runnebaum, R. C.; Brodwater, K. C.; Browning, N. D.; Block, D. E.; Gates, B. C. *Catal. Lett.* **2012**, *142*, 1190−1196.

(13) Nimmanwudipong, T.; Runnebaum, R. C.; Block, D. E.; Gates, B. C. *Energy Fuels* **2011**, *25*, 3417−3427.

(14) Runnebaum, R. C.; Nimmanwudipong, T.; Block, D. E.; Gates, B. C. *Catal. Sci. Technol.* **2012**, *2*, 113−118.

DOI: 10.1021/cs5016244
ACS Catal. 2015, 5, 2423−2435

(15) Bui, V. N.; Toussaint, G.; Laurenti, D.; Mirodatos, C.; Geantet, C. *Catal. Today* **2009**, *143*, 172−178.
(16) Gonzalez-Borja, M. A.; Resasco, D. E. *Energy Fuels* **2011**, *25*, 4155−4162.
(17) Bykova, M. V.; Ermakov, D. Y.; Kaichev, V. V.; Bulavchenko, O. A.; Saraev, A. A.; Lebedev, M. Y.; Yakovlev, V. A. *Appl. Catal., B* **2012**, *113*−*114*, 296−307.
(18) Lausche, A. C.; Falsig, H.; Jensen, A. D.; Studt, F. *Catal. Lett.* **2014**, *144*, 1968−1972.
(19) Newman, C.; Zhou, X. B.; Goundie, B.; Ghampson, I. T.; Pollock, R. A.; Ross, Z.; Wheeler, M. C.; Meulenberg, R. W.; Austin, R. N.; Frederick, B. G. *Appl. Catal., A* **2014**, *477*, 64−74.
(20) Mortensen, P. M.; Grunwaldt, J. D.; Jensen, P. A.; Jensen, A. D. *ACS Catal.* **2013**, *3*, 1774−1785.
(21) Lee, K.; Gu, G. H.; Mullen, C. A.; Boateng, A. A.; Vlachos, D. G. *ChemSusChem* **2015**, *8*, 315−322.
(22) Kresse, G.; Furthmuller, J. *Comput. Mater. Sci.* **1996**, *6*, 15−50.
(23) Kresse, G.; Hafner, J. *Phys. Rev. B* **1993**, *47*, 558−561.
(24) Kresse, G.; Joubert, D. *Phys. Rev. B* **1999**, *59*, 1758−1775.
(25) Perdew, J. P.; Wang, Y. *Phys. Rev. B* **1992**, *45*, 13244−13249.
(26) Perdew, J. P.; Wang, Y. *Phys. Rev. B* **1986**, *33*, 8800−8802.
(27) Grimme, S.; Antony, J.; Ehrlich, S.; Krieg, H. *J. Chem. Phys.* **2010**, *132*, 154104.
(28) Waseda, Y.; Hirata, K.; Ohtani, M. *High Temp. High Pressures* **1975**, *7*, 221−226.
(29) Henkelman, G.; Uberuaga, B. P.; Jonsson, H. *J. Chem. Phys.* **2000**, *113*, 9901−9904.
(30) Henkelman, G.; Jonsson, H. *J. Chem. Phys.* **1999**, *111*, 7010−7022.
(31) Heyden, A.; Bell, A. T.; Keil, F. J. *J. Chem. Phys.* **2005**, *123*, 224101.
(32) Olsen, R. A.; Kroes, G. J.; Henkelman, G.; Arnaldsson, A.; Jonsson, H. *J. Chem. Phys.* **2004**, *121*, 9776−9792.
(33) Lu, J. M.; Behtash, S.; Faheem, M.; Heyden, A. *J. Catal.* **2013**, *305*, 56−66.
(34) Buzzi-Ferraris, G. *BzzMath: Numerical libraries in C++", Politecnico di Milano*; www.chem.polimi.it/homes/gbuzzi.
(35) Liu, W.; Ruiz, V. G.; Zhang, G. X.; Santra, B.; Ren, X. G.; Scheffler, M.; Tkatchenko, A. *New J. Phys.* **2013**, *15*, 053046.
(36) Grabow, L. C.; Hovlbak, B.; Norskov, J. K. *Top. Catal.* **2010**, *53*, 298−310.
(37) Chiu, C. C.; Genest, A.; Borgna, A.; Rosch, N. *ACS Catal.* **2014**, *4*, 4178−4188.
(38) Lu, J.; Heyden, A. *J. Catal.* **2015**, *321*, 39−50.
(39) Campbell, C. T. *J. Catal.* **2001**, *204*, 520−524.
(40) Campbell, C. T. *Top. Catal.* **1994**, *1*, 353−366.
(41) Kozuch, S.; Shaik, S. *J. Am. Chem. Soc.* **2006**, *128*, 3355−3365.
(42) Kozuch, S.; Shaik, S. *J. Phys. Chem. A* **2008**, *112*, 6032−6041.
(43) Stegelmann, C.; Andreasen, A.; Callaghan, C. *J. Am. Chem. Soc.* **2009**, *131*, 8077−8083.

DOI: 10.1021/cs5016244
ACS Catal. 2015, 5, 2423−2435